DOI: 10.1557/adv.2019.96

Selective area growth of $In_xGa_{1-x}As$ nanowires on HfO_2 templates for highly scaled nMOS devices

Paloma Tejedor[1] and Marcos Benedicto[2]

[1]*Instituto de Ciencia de Materiales de Madrid (ICMM), CSIC. Sor Juana Inés de la Cruz 3, 28049-Madrid, Spain.*

[2]*Universidad Pontificia Comillas ICAI-ICADE, Alberto Aguilera 23, 28015-Madrid, Spain.*

ABSTRACT

The replacement of the strained Si channel in metal-oxide-semiconductor-field-effect-transistors (MOSFETs) with high electron mobility III-V compound semiconductors, particularly InGaAs, is being intensively investigated as an alternative to improve the drive current at low supply voltages in sub-10 nm CMOS applications. As device scaling continues, the reduction of the source and drain contact resistance becomes one of the most difficult challenges to fabricate highly scaled III-V-MOSFETs. In this article, we describe a self-aligned process based on selective molecular beam epitaxial regrowth of $In_xGa_{1-x}As$ (x=0-1) raised source/drain nanowire structures on etched recessed areas of a nanopatterned HfO_2 template as a key element to integrate high mobility III-V materials with high-κ dielectrics in three-dimensional device architectures. The interaction of atomic H with the surface of the HfO_2 nanopatterns has been investigated by using AFM, ToF-SIMS, and ARXPS. Selective growth has been observed for all values of x between 0 and 1. AFM results show that atomic H lowers the temperature process window for $In_xGa_{1-x}As$ selective growth. HRTEM images have revealed the conformality of the growth and the absence of nanotrench formation near the HfO_2 mask edges. $In_xGa_{1-x}As$ alloys grown on H-treated HfO_2 patterned substrates exhibit a higher uniformity in chemical composition and full strain relaxation for $x \geq 0.5$.

INTRODUCTION

Metal-oxide-semiconductor field effect transistor (MOSFET) scaling has been the primary means by which the semiconductor industry has achieved unprecedented performance gains during the last few decades. But the improvements attained in the last four technology nodes have relied on the incorporation of high-κ dielectric materials in the gate stack, the use of strain engineering in the transistor channel and the introduction of novel device architectures. Further scaling to the end of the roadmap will require the replacement of the strained Si MOSFET channel (and the source/drain regions) with alternate materials offering a higher potential quasi-ballistic-carrier velocity and higher mobility than Si, integrated in fully-depleted semiconductor-on-insulator (FDSOI) and/or gate-all-around devices [1-3].

The large electron mobility of III-V compounds compared to Si makes these semiconductors very attractive as nMOSFET channel materials for ultimate CMOS. In particular, ternary compound semiconductors like InGaAs, having moderate bandgaps and acceptable energy difference between the lowest and the second lowest conduction band minima are excellent candidates for Si channel replacement. Despite the great advances achieved in the integration of III-V semiconductors on Si substrates [4,5], there are still challenges that must be tackled in order to benefit from the exceptional transport properties of these materials in sub-10 nm devices, such as the realization of low contact resistance self-aligned source/drain access regions [6-8]. A variety of approaches to lower contact resistance in nanoscale III-V devices have been reported to date, including the use of self-aligned molybdenum metal contacts [9], nickel-InGaAs alloys [10,11], digital etching of the III-V semiconductor surface prior to metal deposition [12] or heavy doping with molecular monolayers or co-deposition during III-V epitaxial growth [13,14]. In the present work, we describe a scalable and self-aligned process based on selective molecular beam epitaxial regrowth of InGaAs raised source/drain nanowire structures on etched recessed areas of a HfO2 nanopatterned template that enables the integration of high mobility III-V materials with high-k dielectrics in three-dimensional transistors. Special emphasis has been placed on the impact of atomic H on the process window for III-V selective growth, the nucleation and growth dynamics, the relief of lattice mismatch in the open trenches and the structure and composition of the epilayers grown on the patterned substrates.

EXPERIMENTAL DETAILS

HfO_2 films with a nominal thickness of 10 nm were deposited by ALD on 2 inch diameter GaAs (001) wafers. Nanostructuring of the HfO_2 thin films was carried out by Lloyd´s mirror laser interference lithography using a He-Cd laser (λ=325 nm) and selective plasma etching in CF_4 and O_2.The average HfO_2 linewidth and pitch of the nanopattern were 100 nm and 190 nm, respectively. Prior to epitaxial growth, the nanopatterns were cleaned in UV-O_3 and subsequently heated in the growth chamber to eliminate the native oxide of the open GaAs trenches by thermal desorption at 600ºC or, alternatively, by exposure to an atomic H beam generated *in situ* by dissociation of H_2 gas (99.999% purity) in a home-made cracker cell at a substrate temperature of 400ºC. All $In_xGa_{1-x}As$ samples were grown on the HfO_2/GaAs nanopatterns at temperatures between 400 and 560ºC with a constant V/III flux ratio of 10 at a rate of 0.4 μm/h in a solid-source RIBER Compact-12 III-V MBE system, equipped with a 10 keV electron

gun for reflection high-energy electron diffraction (RHEED) measurements. Elemental Ga and In were supplied by conventional effusion cells, while As_2 was provided by a Mark-V (Veeco) cracker cell.

The surface morphology of all samples was examined with an AFM instrument operating in dynamic mode under ambient conditions. Images were recorded at scans rates of 0.5 lines per second with Si cantilevers having a nominal end radius of 2 nm and a resonance frequency of 75 kHz. A FEI NovaNanoSEM 230 scanning electron microscope was also used to analyze the surface topography of the samples. Mass spectra, elemental maps and depth profiles of the HfO_2/GaAs samples were acquired in dual-beam mode, using a ToF-SIMS IV instrument, equipped with an sputter gun used to generate 1.0 keV Cs^+ ions and a 25 keV Bi^{3+} liquid metal ion gun (LMIG) as the primary ion source for analysis. The stoichiometry of the HfO_2 layers after exposure to the atomic H beam was studied by ARXPS. Cross-sectional specimens suitable for HR-TEM were prepared using a focused ion beam (FIB) FEI Strata 400 STEM dual-beam system and examined in a Philips Tecnai F20 TEM/STEM microscope operating at 200 keV and equipped with an integrated system for energy dispersive spectroscopy (EDS) analysis. Bright field TEM images were recorded.

RESULTS AND DISCUSSION

Figures 1a and 1b show SEM images of the resist nanopattern and the final HfO_2/GaAs nanostructured template morphology, where ~90 nm wide etched GaAs trenches for selective growth can be observed. AFM measurements rendered rms values of 0.14 nm and 0.18 nm for the HfO_2 and GaAs surface roughness (rms), respectively.

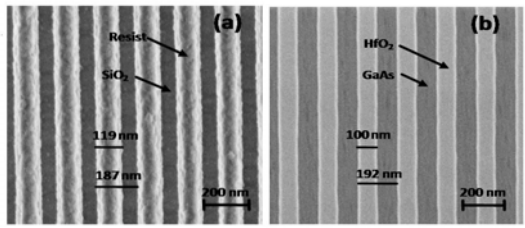

Figure 1. Scanning electron micrographs of the resist pattern and the resulting nanostructured HfO_2/GaAs substrate after selective CF_4 and O_2 plasma etching.

ToF-SIMS analysis of the HFO_2/GaAs templates after exposure to atomic H as a function of the H_2 gas flow rate (0.1-0.3 sccm) introduced into the growth chamber and the substrate temperature indicated that between 350 and 400ºC the HfO_2 is etched layer-by-layer and the surface reaction has an associated activation energy of ~23 Kcal/mol. Depth profiles of the main impurities present on the HfO_2 thin layer, i.e., C, Cl, F, and S, show a general concentration decrease with increasing temperature, as illustrated in Figure 2. ARXPS spectra (not shown here) confirmed that the HfO_2 surface stoichiometry is preserved under the temperatures and gas flow rates here studied. AFM imaging showed that smooth HfO_2 surface morphologies with rms values below 0.2 nm were favoured by hydrogen flow rates ≥0.3 sccm. In consequence, cleaning of the HfO_2/GaAs templates with atomic H prior to InGaAs MBE growth was carried out at a substrate temperature of 400ºC with a hydrogen flow rate of 0.3 sccm.

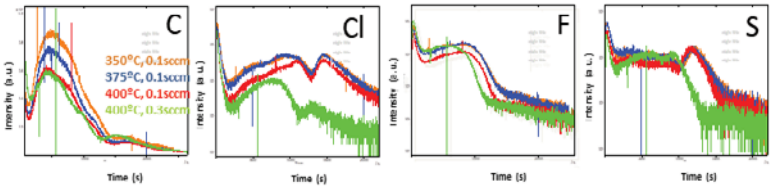

Figure 2. ToF-SIMS depth profiles of C, Cl, F, and S showing the variation of their concentration on the HfO_2 thin layer after exposure to an atomic H beam at different substrate temperatures and H_2 flow rates.

In order to study the impact of chemisorbed H on the InGaAs growth selectivity on the nanostructured templates, three series of samples were prepared at growth temperatures between 400 and 560ºC by (i) thermal desorption of the GaAs native oxide and conventional MBE growth, (ii) atomic H surface cleaning followed by conventional MBE growth, and (iii) atomic H surface cleaning followed by H-assisted MBE growth. Analysis of the surface morphology as a function of growth temperature for each of these methodologies showed that the window for selective growth shifted towards lower temperatures as the exposure time to the atomic H beam was increased. Figure 3a illustrates this variation, attributed to the lower nucleation energy of the III-V compound on the H-terminated GaAs (001) surface and to the lower sticking coefficient of Ga and In adatoms on the H-terminated HfO_2 surface, which prevents the nucleation of InGaAs on the mask. Figure 3b shows a 2.5x2.5 µm AFM image of InGaAs nanowires nucleated on the nanostructured template at 500ºC by conventional MBE growth.

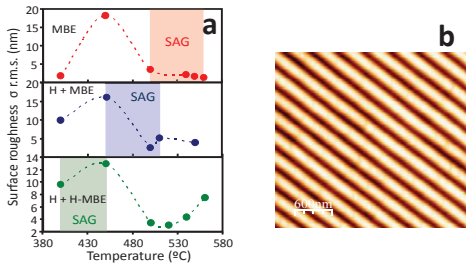

Figure 3. (a) Variation of $In_{0.5}Ga_{0.5}As$ surface roughness measured by atomic force microscopy as a function of growth temperature for the three methodologies described in the text. The coloured regions show the temperature window for selective area growth (SAG) corresponding to each methodology. (b) AFM image of selectively grown InGaAs nanowires at a substrate temperature of 500ºC.

The SEM micrographs in Figure 4 illustrate the surface morphology evolution with nominal thickness of InGaAs grown at 500ºC by conventional MBE on an HfO_2/GaAs template cleaned with atomic H for 30 min. Nucleation of three-dimensional (3D) InGaAs islands on the GaAs trenches occurs initially on the GaAs trenches by the so-called Stranski-Krastanov mechanism (Figure 4a). As growth continues the 3D islands coalesce covering the entire trench to form a nanowire (Figure 4b). With further InGaAs deposition, epitaxial lateral overgrowth on the mask occurs and {011} facets develop (Figure 4c) due to the lower incorporation rates of Ga and In adatoms to the (001) surface with respect to the (100) one: The concentration gradient induces the adatom migration towards the (001) mesa, where they incorporate preferentially, thus leading to the predominance of {011} facets.

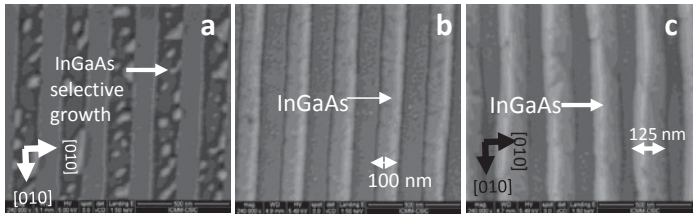

Figure 4. High resolution scanning electron micrographs (HR-SEM) of the surface morphology after deposition of (a) 5 nm, (b) 25 nm and (c) 50 nm (nominal thickness) $In_{0.5}Ga_{0.5}As$ at 500ºC, showing the nucleation and growth of nanowires on the H-terminated HfO_2/GaAs (001) nanopatterns.

Figure 5a shows a cross-section TEM (bright field) micrograph of the self-aligned raised source/drain structure formed after deposition of 25 nm $In_{0.5}Ga_{0.5}As$ on the H-cleaned HfO_2 template. Growth in the trenches is highly conformal and does not lead to nanotrench formation next to the HfO_2 mask edges, a defect associated with leakage currents that has been previously reported for epitaxial micron-scale raised source/drain structures by other authors [15]. Figure 5b depicts a HR-TEM image of the InGaAs nanowire cross-section and its corresponding fast Fourier transform (FFT), equivalent to the electron diffraction pattern. The estimated lattice parameter from the (220) and (200) reflection peaks is 5.8489 Å in both directions, which indicates that the lattice is fully relaxed. The value of the lattice parameter obtained corresponds to a 48% In content, which is in good agreement with the $In_{0.5}Ga_{0.5}As$ nominal composition of the sample. The HR-TEM cross-section image (bright field) shown in Figure 5c illustrates the array of misfit dislocations formed at the InGaAs/GaAs interface during the nucleation stage to relief the lattice strain of the ternary compound. The same behaviour has been observed for $In_xGa_{1-x}As$ alloys with In contents greater than 50%. Elemental profiles of the nanowires determined with the energy dispersive spectrometer (EDS) detector of the scanning TEM microscope revealed that above a 3nm thick transition layer (formed by In-poor $In_xGa_{1-x}As$) the In content does not show any significant variation in the growth direction, contrary to those samples grown by conventional MBE, where In segregation towards the surface typically occurs. This effective reduction of the In diffusion length

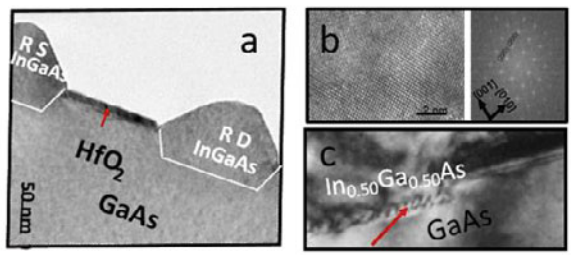

Figure 5. Cross-section transmission electron micrographs (TEM) (bright field) showing (a) the self-aligned raised $In_{0.5}Ga_{0.5}As$ source/drain extended regions selectively grown at 500ºC on the etched recessed trenches adjacent to the HfO_2 gate, (b) a high resolution image of the $In_{0.5}Ga_{0.5}As$ nanowire with its corresponding electron diffraction pattern (FFT) and (c) detail of the array of misfit dislocations formed at the $In_{0.5}Ga_{0.5}As$ /GaAs interface

can be attributed to the surfactant effect of atomic H and its role as catalyst of the direct reaction between chemisorbed Ga-H and In-H monomers and AsH_x precursor species [16].

CONCLUSIONS

We have developed a self-aligned process based on selective epitaxial growth of $In_xGa_{1-x}As$ source/drain regions on etched recessed areas adjacent to a nanopatterned HfO_2 gate using conventional and atomic H-assisted MBE. In-situ cleaning with atomic H prior to epitaxial growth effectively reduces the concentration of the major impurities on the HfO_2 surface, preserving the oxide stoichiometry. The use of atomic H lowers the temperature process window for selective growth due to the reduced activation energy for nucleation on the H-terminated GaAs (001) surface and the blocking of the HfO_2 surface active sites by H. Furthermore, it leads to $In_xGa_{1-x}As$ regrown regions with uniform chemical composition and full strain relaxation for $x \geq 0.5$, enabling its application as source/drain (and channel) material in highly scaled nMOS devices.

Acknowledgments

This work was financially supported by MINECO under grant No. TEC2016-78433, by CSIC under grant No. 201880E058, and by the H2020 European Institute of Innovation & Technology under grant No. EIT15065 (OPTNEWOPT)

References

1. T. Skotnicki, J.A. Hutchby, T. King, H.S.P. Wong, and F. Boeuf, IEEE Circuits Devices Mag. **1**, 16–26 (2005).
2. J.A. del Alamo, Nature **479**, 317 (2011).
3. A.P. Jacob, R. Xie, M.G. Sung, L. Liebmann, R.T.P. Lee, and B. Taylor, International Journal of High Speed Electronics and Systems **26**, 1740001 (2017).
4. K. Tomioka, J. Motohisa, S. Hara, and T. Fukui, Nano Lett. **8**, 10 3475-3480 (2008).
5. N. Waldron, C. Merckling, L. Teugels, P. Ong, F. Sebaai, K. Barla, N. Collaert, and V.-Y. Thean, Solid-State Electron. **115**, 81-91 (2016).
6. S. Masudy-Panah, Y. Wu, D. Lei, A. Kumar, Y.-C. Yeo, and X. Gong, J. Appl. Phys. **123**, 024508 (2018).
7. R.T.P. Lee, W.Y. Loh, R. Tieckelmann, T. Orzali, C. Huffman, A. Vert, G. Huang, M. Kelman, Z. Karim, C. Hobbs, R.J.W. Hill, and S.S.P. Rao, ECS Trans. **66**, 125-134 (2015).
8. A. Veloso, A. De Keersgieter, P. Matagne, N. Horiguchi, and N. Collaert, Mater. Sci. Semicond. Process. 62, 2-12 (2017).
9. X. Zhang, H.X. Guo, Z. Zhu, X. Gong, and Y.C. Yeo, Solid State Electron. 84, 83–89 (2017).
10. S.H. Kim, M. Yokoyama, N. Taoka, R. Iida, S. Lee, R. Nakane, Y. Urabe, N. Miyata, T. Yasuda, H. Yamada, et al. in *Proceedings of the International Electron Devices Meeting (IEDM)*, (IEEE, San Francisco, CA, 2010) pp. 596–599.
11. L. Czornomaz, M. El Kazzi, M. Hopstaken, D. Caimi, P. Mächler, C.Rossel, M. Bjoerk, C. Marchiori, H. Siegwart, and J. Fomperyne, Solid-State Electron. **74**, 71-76 (2012).
12. F. Ravaux, I. Saadat, and M. Jouiad, Crystals **7**, 177 (2017).
13. K.S. Jones, A.G. Lind, C. Hatem, S. Moffatt, and M.C. Ridgeway, ECS Trans. **53**, 97–105 (2013).
14. J. O'Connell, E. Napolitani, G. Impellizzeri, C. Glynn, G.P. McGlacken, C. O'Dwyer, R. Duffy, and J.D. Holmes, ACS Omega, **2**, 1750–1759 (2017).
15. G.J. Burek, M.A. Wistey, U. Singuisetti, A. Nelson, B.J. Thibeault, S.R. Bank, M.J.W. Rodwell, and A.C. Gossard, J. Crys. Growth **311**, 1984-1987 (2009).
16. L. Diez-Merino and P. Tejedor, J. Appl. Phys. **110**, 013106 (2011).